High-Resolution γ-Ray Radiography Produced by a Laser-Plasma Driven Electron Source

Y. Glinec,[1] J. Faure,[1] L. Le Dain,[2] S. Darbon,[2] T. Hosokai,[3] J. J. Santos,[1] E. Lefebvre,[2] J. P. Rousseau,[1] F. Burgy,[1] B. Mercier,[1] and V. Malka[1,*]

[1]*Laboratoire d'Optique Appliquée-ENSTA, UMR 7639, CNRS, École Polytechnique, 91761 Palaiseau, France*
[2]*CEA Ile-de-France, BP 12, 91680 Bruyères-le-Châtel, France*
[3]*Nuclear Engineering Research Laboratory, University of Tokyo, 22-2 Shirane-shirakata, Tokai, Naka, Ibaraki, 319-1188, Japan*

(Received 20 July 2004; published 18 January 2005)

An electron beam from a laser-plasma accelerator is converted into a γ-ray source using bremsstrahlung radiation in a dense material. The γ-ray beam has a pointlike source size because it is generated by a high quality electron beam with a small source size and a low divergence. Using this γ-ray source, the radiography of complex and dense objects with submillimeter resolution is performed. It is the first evidence of a γ-ray source size of a few hundreds micrometers produced with laser-driven accelerators. This size is consistent with results from Monte Carlo simulations.

DOI: 10.1103/PhysRevLett.94.025003 PACS numbers: 52.38.Kd, 41.85.Ja, 87.59.Bh

The interaction of a high-intensity short laser pulse with an underdense plasma produces large electric fields which can be used to accelerate electrons. Since the medium is already ionized, the electric field amplitude is several orders of magnitude [1] greater than those currently attainable with conventional accelerator technology, which is now limited by material breakdown. Because of the rapid evolution of laser technology, leading to performance enhancement for a decreasing cost, laser-plasma interaction is expected to play an important complementary role in future generations of particle accelerators. Among the different laser-driven acceleration mechanisms (direct laser acceleration [2], plasma beat wave accelerator [1,3–5], self-modulated laser wakefield accelerator [6–10]), the forced laser wakefield regime was reported recently in our laboratory [11]. Here, the nonlinear behavior of the plasma wave drives the generation of energetic and low emittance electron beams [12]. The electron source diameter is also directly comparable to the laser waist (18 μm). This is an asset compared to conventional accelerators with similar electron energy, where the electron beam emittance hinders the beam focusing below millimeter scale. In this Letter, we take advantage of these recent improvements in laser-plasma electron accelerators to generate a high quality γ-ray source, which is obtained by bremsstrahlung radiation of electrons slowing down in a conversion target with high atomic number. In previous work on laser-driven radiography, no attention was given to precisely measure the γ-ray source size [13,14]. In the present Letter, radiographies of complex dense objects are performed, giving evidence of this small γ-ray source size. The results are then correlated to Monte Carlo simulations. It is a promising source for nondestructive material or mechanical inspection [15] and it could also play an important role in clinical applications [16] or in research fields where the size of the γ-ray source must be reduced.

The experiment is performed on the Ti:sapphire laser in ''salle jaune'' at Laboratoire d'Optique Appliquée, which operates in chirped-pulse amplification mode at 820 nm [17]. The laser delivers 30 fs at full width at half maximum (FWHM) linearly polarized pulses with on-target energies of 1.3 J. The laser beam is focused with an $f/18$ off axis parabolic mirror onto a sharp-edged, constant density profile, 3 mm-diameter supersonic helium gas jet, which provides an initial plasma electron density n_e of 7.5×10^{18} cm^{-3}. The waist of the focal spot is 18 μm, resulting in vacuum focused intensities of the order of 4×10^{18} W/cm^2, which corresponds to a normalized laser vector potential, $a_0 = eA/m_e c^2$, of 1.4.

The electron spectrum, shown in Fig. 1, is measured in one shot by imaging the light emitted by a Lanex film, which is the relaxation transition of a phosphor excited by the electrons passing through the material. This film is placed on the laser axis, behind compact magnets, and it is protected from direct laser light by a thin aluminum foil. This spectrum is calibrated using an Integrating Current Transformer (ICT), centered on the laser axis, which gives

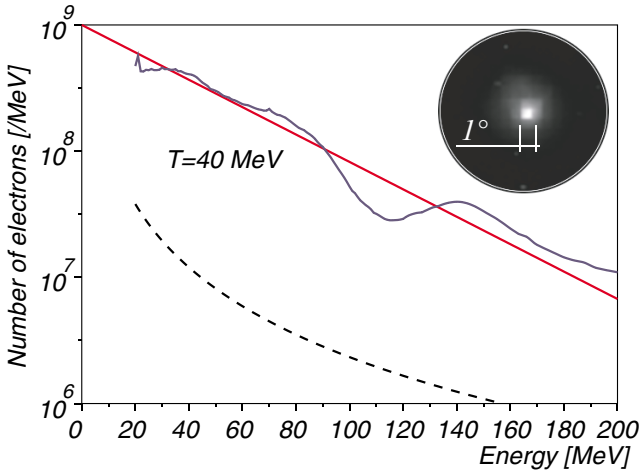

FIG. 1 (color online). Electron spectrum, fitted by a Maxwellian distribution with temperature $T = 40$ MeV, and electron dose profile in the Lanex film in the inset. The dashed curve is the detection threshold.

the charge of the collected electrons (whose energy is above 110 MeV). The signal on the film is well above the detection threshold, and the minimal (20 MeV) and maximal (200 MeV) energy which are represented are limited by the resolution of the spectrometer. A Maxwellian fit of the spectrum corresponds to an average temperature of $T = 40$ MeV. When removing the magnets, we obtain the dose deposition profile of the electron beam, which is shown to be in a narrow cone of 1° FHWM in the inset of Fig. 1, and we also measure the total charge of the electron beam passing through the ICT. The number of electrons with energy above 2 MeV was found to be about 10^{10} per shot.

The experimental setup for radiography is drawn on Fig. 2. This characterized electron source is converted into γ rays inside a 2.5 mm-thick tantalum converter, placed at 3 mm from the center of the nozzle. The bremsstrahlung radiation produced during the scattering inside the foil is used to radiograph a 20 mm-diameter spherical hollow object made of tungsten, located 220 mm away from the nozzle. A sinusoidal shape, with cylindrical symmetry, is etched on the inner part of the object, as shown on Fig. 2. For the upper (lower) part of the object, respectively, each oscillation of the 6-period (5-period) sinusoid corresponds to an 11° (13°) rotation angle and an amplitude of 1.9 mm (2.4 mm). The average radius of this sinusoid from the center is 7.85 mm on the A-A′ cut, which gives a maximum thickness of 12.9 g/cm^2. The axis of this object is chosen perpendicular to the laser axis. The transmitted radiation is then detected on a γ camera, composed of a Bismuth-Germanium-Oxyde (BGO) scintillator which is imaged on a charge-coupled device (CCD) camera. The imaging system is composed of a flat mirror, an objective, and a photon amplifier. The size of each BGO crystal (600 μm) in the 160 mm-square matrix limits the resolution of the detector. The scintillator is placed at 1.6 m from the electron source. This makes a magnification factor of 7.3, corresponding to a pixel size of 80 μm on the object. The choice of this magnification is the result of a compromise between decent spatial resolution and a high enough dose on the γ camera. The nozzle-object distance is chosen large enough to reduce the parallelism problems which would blur small details on the image. In order to avoid bremmstrahlung of electrons inside the object which is radiographed, a magnetic field is applied behind the converter to bend the electron trajectory. Without the converter, only electrons with kinetic energy above 60 MeV are expected to hit the object. We have also added a 7.5 mm-thick aluminum foil in order to increase the scattering of the electrons. The magnets combined with the aluminum foil ensure an efficient electron scattering as well as the reduction of the noise generated inside the object.

In order to evaluate the characteristics of the photon source, Monte Carlo (MC) simulations were performed using GEANT4 [18] and MCNP [19]. In order to reduce the computing time, a total of 10^8 electrons are simulated and distributed along a Maxwellian energy distribution $f(E) \propto \exp(-E/T)$ and a Gaussian angular distribution $g(\Theta) \propto \exp(-4\ln 2\Theta^2/\Theta_0^2)$, whose aperture $\Theta_0 = 1°$ FWHM was chosen to be independent of the electron energy. In both cases, the MC simulations described two kinds of discrete events: (i) elastic scattering [20] of the electrons on the atoms of a pure, homogeneous, invariant material and, (ii) photon production above an arbitrary threshold of $k_{\mathrm{cut}} = 10$ keV [21]. Between these impacts, the collisional stopping power [22] and the radiative stopping power [23], corresponding to all photons with energy $k < k_{\mathrm{cut}}$, absorbed in the surrounding material, were calculated to

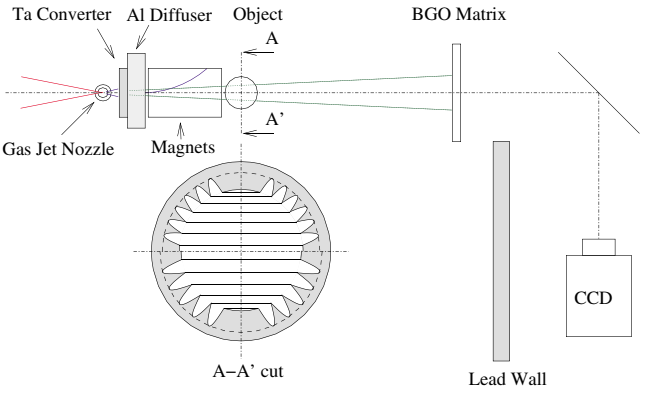

FIG. 2 (color online). Experimental setup. The electrons accelerated during the interaction of the laser pulse with the gas jet slow down in the tantalum converter, which leads to γ-ray generation. The electrons are removed from the laser axis by strong magnets and the aluminum diffuser. The intensity transmitted through the object is imaged on the γ camera. A cut of the object is also shown.

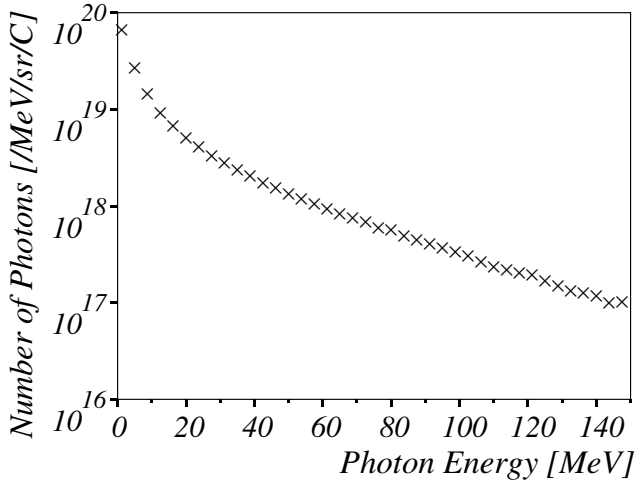

FIG. 3. Photon spectrum from Monte Carlo simulation averaged between 0° and 1° (with parameters $T = 40$ MeV and $\Theta_0 = 1°$ for the electron beam converted in γ rays in a 2.5 mm-thick tantalum target followed by a 7.5 mm-thick aluminum foil).

account for the energy loss in the medium along the electron trajectory. The results of the electron transport and γ-ray production in a foil are presented in Fig. 3 and 4. They show a very well collimated ($\sim 3°$ FWHM), energetic distribution for this photon source.

From the simulations, the photon source size is $320 \pm 10\mu$m in diameter (FWHM) at the output of the tantalum converter. Since the cross sections scale as the square of the atomic number, the radiation conversion in the aluminum foil is expected to be low compared to the yield in the converter. According to the simulations, the incident electron energy conversion is 49% in the first converter and 2.8% in the second one. So, the aluminum filter does not significantly degrade the γ-ray source. For a monoenergetic photon beam, the exact definition of the spot size is defined as the minimum rms diameter of the γ-ray flux, computed using ray-tracing methods in all planes along the laser axis [24]. To extend this definition to polychromatic beams, the contribution of each photon is weighted with its attenuation coefficient in the detector, and the minimum rms diameter of this modified flux must be computed. In this simulation, the dose distribution size was calculated in one plane (the tantalum output plane). This value should be close to the "effective" γ-ray source size, located somewhere inside the converter. A radiography of an object with sharp edges was also performed in order to estimate the experimental spot size. Figure 5 is comparable to images obtained by knife-edge techniques. In this case, we use a thick 20 mm steel plate with squares of different size drilled in it. Because of the manufacturing process, lines between the sets of 5 squares of different sizes can also be seen on the image. The value which is measured on Fig. 5 is the FWHM size of the derivative of the plot profile averaged over 5 lines. This gives a size of 31 ± 1 pixels on the CCD camera which corresponds to a source size of $450 \pm 15\mu$m FWHM. The mismatch with the computed value is due to the following factors: (i) the intrinsic detector blur ($\sim 170\ \mu$m in the object plane), which was not taken into account in the simulation, (ii) the alignment of the 20 mm-thick plate, which must be perfectly perpendicular to the laser axis, (iii) the initial parameters of the simulation which are slightly different from the experimental electron beam. In particular, the angular divergence is expected to be larger for low energies, thus increasing the γ-ray spot size. Finally, (iv) the scattered electrons may also interact with the object itself, adding noise to the radiography. However, it should be kept in mind that the spatial quality of the γ-source can still be enhanced by moving the converter towards the nozzle, on the laser axis, or by decreasing the converter thickness or even by using stronger magnets to avoid using aluminum foils.

From the same calculations, the expected γ dose on the laser axis at 1 m in air should be about 4.5×10^5 Gy/C without the object. In other terms, for a total charge of 1.6 nC (above 2 MeV), this would make a photon dose of 1 Gy in air at 2.7 cm from the gas jet nozzle.

The output of this MC simulation was used as a photon source for a radiography simulation. The intensity I_k of photons was damped according to the thickness of material in the object l using a Beer-Lambert law, $I_k(l) \propto \exp[-\mu(k)l]$, where $\mu(k)$ is the γ-ray attenuation coefficient from the NIST database [25] corresponding to photon energy k. A map of thicknesses was calculated by projecting the object in the (x, y) plane, using a ray-tracing technique throwing rays from a point source located in the middle of the gas jet. The intensity attenuation rate is 54% for 10 MeV photons traveling through 12.9 g/cm^2.

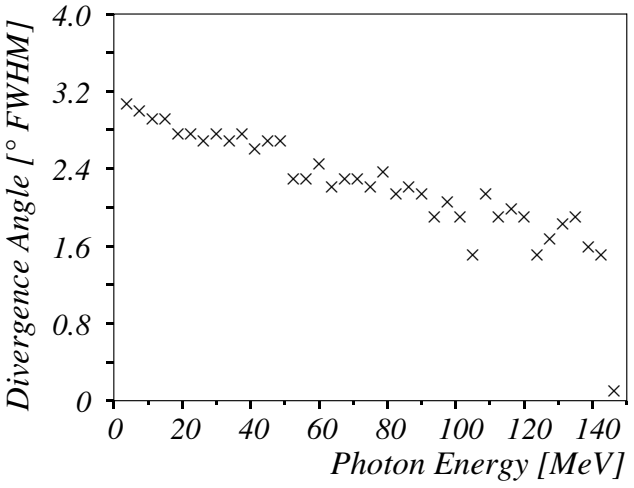

FIG. 4. Angular distribution of photons computed by Monte Carlo simulation (with parameters of Fig. 3).

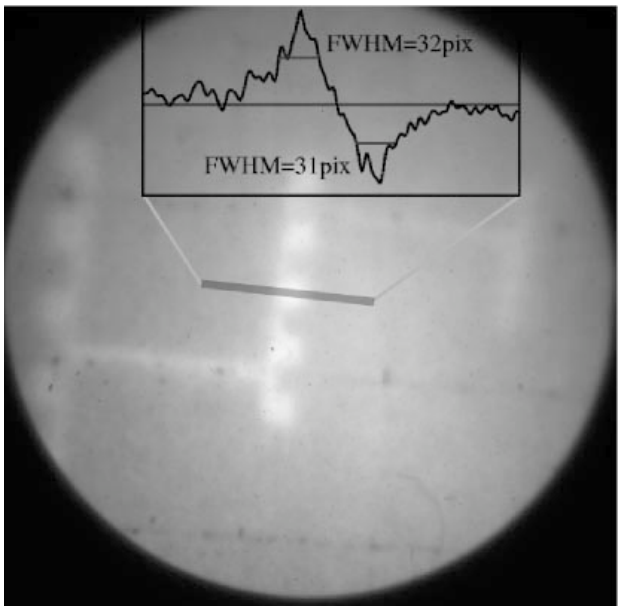

FIG. 5. Spot size measurement. This object is a 20 mm-thick steel plate, with 1.0, 0.75, and 0.4 mm-square holes from left to right. The curve represents the derivative of the profile averaged over the rectangular area in the center.

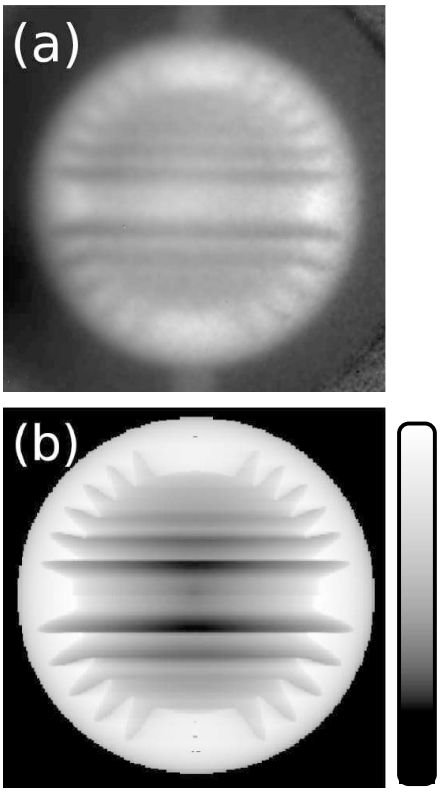

FIG. 6. Radiography images of a 2 mm-diameter tungsten object with cylindrical symmetry corresponding to (a) the experimental image and (b) the computed image. Color tables are linear. A simple post processing has been performed, consisting of a division by a reference image without the object.

The incidence of photons (up to 2.6°) is taken into account in the radiography simulation, leading to a blurring of the calculated contrast as the radius increases. The discrete events for the photons (photoelectric effect, Compton effect, pair production) are not simulated. Therefore, the secondary photons are not described. The experimental and computed radiographs are presented in Fig. 6. One can notice that all sinusoidal lobes can be seen on the experimental image. A detailed analysis of this radiograph will be presented in another publication. The simulation shows the maximum contrast that could be obtained, independently of the experimental limitations described above.

In conclusion, we performed a submillimetric resolution radiography experiment using a laser-driven electron accelerator. The main characteristics of this electron beam were used in a MC simulation to calculate the properties of the γ-ray source produced by bremsstrahlung radiation inside a tantalum converter. From the MC simulations, and from the experimental image, we calculated and measured a spot size which should be about 320 μm FWHM numerically and less than 450 μm FWHM experimentally. This photon source is also expected to be ultrashort since the electron source duration is comparable to the laser pulse duration (30 fs) and the lengthening during scattering in the tantalum target is controlled by its thickness. Ultrashort γ-ray sources are interesting for several applications including fast moving object monitoring or high density metal compression visualization [15]. To conclude, these electrons and γ sources have a better spatial and temporal resolution than other conventional sources. Recent major improvements in laser-plasma acceleration have also shown the production of monoenergetic electron beams [26–28]. All these excellent characteristics, combined with a decreasing cost and size of terawatt lasers, will make such sources extremely useful for radiographic applications.

*Electronic address: victor.malka@ensta.fr

[1] T. Tajima and J. Dawson, Phys. Rev. Lett. **43**, 267 (1979).
[2] C. Gahn *et al.*, Phys. Rev. Lett. **83**, 4772 (1999).
[3] E. Esarey, P. Sprangle, J. Krall, and A. Ting, IEEE Trans. Plasma Sci. **24**, 252 (1996), and references therein.
[4] F. Amiranoff *et al.*, Phys. Rev. Lett. **68**, 3710 (1992).
[5] C. E. Clayton, M. J. Everett, A. Lal, D. Gordon, K. A. Marsh, and C. Joshi, Phys. Plasmas **1**, 1753 (1994).
[6] A. Modena *et al.*, Nature (London) **377**, 606 (1995).
[7] E. Esarey, J. Krall, and P. Sprangle, Phys. Rev. Lett. **72**, 2887 (1994).
[8] N. E. Andreev, L. M. Gorbunov, V. I. Kirsanov, A. A. Pogosova, and R. R. Ramazashvili, JETP Lett. **55**, 571 (1992).
[9] T. M. Antonsen and P. Mora, Phys. Rev. Lett. **69**, 2204 (1992).
[10] P. Sprangle, E. Esarey, J. Krall, and G. Joyce, Phys. Rev. Lett. **69**, 2200 (1992).
[11] V. Malka *et al.*, Science **298**, 1596 (2002).
[12] S. Fritzler *et al.*, Phys. Rev. Lett. **92**, 165006 (2004).
[13] M. D. Perry *et al.*, Rev. Sci. Instrum. **70**, 265 (1999).
[14] R. D. Edwards *et al.*, Appl. Phys. Lett. **80**, 2129 (2002).
[15] Y. Chen *et al.*, in *Proceedings of the XXI International Linac Conference, Gyeongju, Korea*, (U. S.Department of Energy, 2002).
[16] K. K. Kainz *et al.*, Med. Phys. **31**, 2053 (2004).
[17] M. Pittman, S. Ferré, J.-P. Rousseau, L. Notebaert, J. P. Chambaret, and G. Chériaux, Appl. Phys. B **74**, 529 (2002).
[18] S. Agostinelli *et al.*, Nucl. Instrum. Methods Phys. Res., Sect. A **506**, 250 (2003).
[19] F. B. Brown *et al.*, Trans. Am. Nucl. Soc. **87**, 273 (2002).
[20] E. Zeitler and H. Olsen, Z. Naturforsch. **B21**, 1321 (1966).
[21] M. Seltzer and J. Berger, At. Data Nucl. Data Tables **35**, 345 (1986).
[22] F. Rohrlich and B. C. Carlson, Phys. Rev. **93**, 38 (1954).
[23] A. Bielajew, National Research Council of Canada Report No. PIRS-0203, 1989.
[24] G. W. Forbes, J. Opt. Soc. Am. A **5**, 1943 (1988).
[25] J. H. Hubbel and S. M. Seltzer, National Institute of Standards and Technology, Gaithersburg, MD Report No. NISTIR 5632, 1997.
[26] J. Faure *et al.*, Nature (London) **431**, 541 (2004).
[27] C. G. R. Geddes *et al.*, Nature (London) **431**, 538 (2004).
[28] S. Mangles *et al.*, Nature (London) **431**, 535 (2004).